Biomaterials 35 (2014) 2971–2980

Contents lists available at ScienceDirect

Biomaterials

journal homepage: www.elsevier.com/locate/biomaterials

Quantitative assessment of Tn antigen in breast tissue micro-arrays using CdSe aqueous quantum dots

Giang H.T. Au [a], Linette Mejias [b], Vanlila K. Swami [b], Ari D. Brooks [c], Wan Y. Shih [a], Wei-Heng Shih [d,*]

[a] School of Biomedical Engineering, Science and Health System, Drexel University, 3141 Chestnut Street, Philadelphia, PA 19104, USA
[b] Department of Pathology and Laboratory Medicine, College of Medicine, Drexel University, 245 N. 15th Street, Philadelphia, PA 19102, USA
[c] Department of Surgery, College of Medicine, Drexel University, 245 N. 15th Street, Philadelphia, PA 19102, USA
[d] Department of Materials Science and Engineering, Drexel University, 3141 Chestnut Street, Philadelphia, PA 19104, USA

ARTICLE INFO

Article history:
Received 15 November 2013
Accepted 13 December 2013
Available online 8 January 2014

Keywords:
Immunochemistry
Image analysis
Nanoparticle
Quantum dots
Breast cancer
Surgery margin

ABSTRACT

In this study, we examined the use of CdSe aqueous quantum dots (AQDs) each conjugated to three streptavidin as a fluorescent label to image Tn antigen expression in various breast tissues via a sandwich staining procedure where the primary monoclonal anti-Tn antibody was bound to the Tn antigen on the tissue, a biotin-labeled secondary antibody was bound to the primary anti-Tn antibody, and finally the streptavidin-conjugated AQDs were bound to the biotin on the secondary antibody. We evaluated the AQD staining of Tn antigen on tissue microarrays consisting of 395 cores from 115 cases including three tumor cores and one normal-tissue core from each breast cancer case and three tumor cores from each benign case. The results indicated AQD-Tn staining was positive in more than 90% of the cells in the cancer cores but not the cells in the normal-tissue cores and the benign tumor cores. As a result, AQD-Tn staining exhibited 95% sensitivity and 90% specificity in differentiating breast cancer against normal breast tissues and benign breast conditions. These results were better than the 90% sensitivity and 80% specificity exhibited by the corresponding horse radish peroxidase (HRP) staining using the same antibodies on the same tissues and those of previous studies that used different fluorescent labels to image Tn antigen. In addition to sensitivity and specificity, the current AQD-Tn staining with a definitive threshold was quantitative.

1. Introduction

Immunostaining is an integral part of pathological analysis for diagnostic and therapeutic decisions and monitoring [1,2]. Immunostaining is used to visualize cellular or tissue constituents (antigens) based on antigen–antibody interactions. Two main staining methods in immunostaining are immunohistochemical (IHC) staining which uses an enzyme such as horse radish peroxidase (HRP) to react with its substrate to produce a colored substance to show the molecules of interest and immunofluorescence (IF) which uses fluorescent molecules to light up the molecules of interest. HRP-labeled antibodies are widely used in pathological examination due to the stability and durability of the staining over a long period of time. However, the extent of the expression of the biomarkers often requires semi-quantitative evaluation. Many factors can affect the assessment including different scoring systems, amount of chemicals, etc. Determination of whether a tissue is positive or negative often depends on the experience and skill of the interpreter, possibly leading to inaccurate results. Since the late 1980s, computerized image analysis systems have been introduced and shown to be a more accurate means to quantify the image. However, the non-linear relationship that occurs at higher levels between the amount of the antigen and the absorption intensity of the chromogen used in HRP-IHC, diaminobenzidine (DAB), can result in inaccurate interpretations [1,3]. It remains a challenge to quantify HRP-IHC accurately. Recent approaches have explored the use of IF-based methods and fluorescent microscopy to better quantify protein expression in tissues [4,5]. Conventional organic fluorescent dyes have several limitations such as small Stokes shifts and difficulty in distinguishing positive fluorescent signals from auto-fluorescence of formalin-fixed-and-paraffin-embedded tissues [6]. Moreover, photo-bleaching is a major drawback of conventional fluorescent dyes which makes it difficult if not impossible to view the same region repeatedly [7].

Semiconductor nanoparticles such as quantum dots (QDs) are a new class of inorganic fluorophores that are made of inorganic

* Corresponding author.
E-mail address: shihwh@drexel.edu (W.-H. Shih).

0142-9612/$ – see front matter © 2013 Elsevier Ltd. All rights reserved.
http://dx.doi.org/10.1016/j.biomaterials.2013.12.034

materials. They exhibit high fluorescence intensity, high resistance to photo-bleaching [8] and a wide range of possible emission wavelengths. Their size is between 2 and 10 nm, which is comparable to green fluorescent protein (GFP) [9]. By changing the particle size of the same material, the emission wavelength is tunable making it possible to image multiple markers simultaneously on the same pathological sites [10]. They have the potential to be an excellent fluorescent molecular probe to image biomolecules when combined with specific receptors to the biomolecules of interest. Bioimaging applications of QDs have been demonstrated in cell labeling and tracking [11,12], cell proliferation [13], *in vivo* sentinel lymph node mapping in a pig [14], *in vivo* brain imaging in mice [15], molecular beacons for DNA detection [16–18] and *in vivo* tumor detection in mice [19,20]. For specific imaging of a target antigen, QDs can be coupled with an antibody to detect the target antigen on the cell surface. Recent studies have demonstrated such QD-based IF staining in molecular pathology for HER2 expression in breast cancer tissues [21,22]. The advantages of such QD-based IF staining for molecular pathology include brighter fluorescent signals over organic dyes, therefore, a better signal-to-noise ratio, and better detection sensitivity and accuracy than conventional IHC [21,23].

However, commercial QDs are made in an organic solvent (OQDs hereafter). To be used in bioimaging, OQDs must undergo solvent and ligand exchange. The intrinsic disadvantage of such solvent and ligand exchange is that the amount of capping molecules on the OQDs is insufficient for optimal colloidal stability and biomolecule conjugation. Typically, a large amount of proteins [24] must be used in order to bind the protein on the OQDs, rendering OQD IF staining not cost-effective. We have pioneered an aqueous synthesis process in which QDs can be made directly in water with 3-mercaptopropionic acid (MPA) as the capping molecule [24–28] (Aqueous quantum dots (AQDs) hereafter). Using such approach, we have made bright MPA-capped CdSe AQDs from a nominal MPA:Cd:Se = 4:3:1 with a high quantum yield of 70% [24]. Furthermore, these CdSe AQDs could conjugate to streptavidin (SA) with a high SA-conjugation efficiency of 75% (i.e., 75 of every 100 SA molecules in the solution were conjugated to AQDs) to form a SA-AQD complex consisting of one AQD with 3.4 SA with high imaging efficacy [24] as opposed to a 3% SA-conjugation efficiency exhibited by OQDs to form a SA-OQD complex consisting of one OQD with 2.7 SA with similar imaging efficacy [24]. These results illustrated that AQDs needed only one twentieth of the SA needed by OQDs to achieve the same imaging efficacy [24]. As protein is typically the cost limiting factor, AQDs' ability to conjugate to SA with high SA conjugation efficacy offers great potential to use AQDs for cost-effective IF staining in molecular pathology applications.

The goal of this study is to examine the efficacy of CdSe AQD-based IF imaging method for molecular pathology applications. Specifically, we will use CdSe AQDs to image Tn antigen, a pan-carcinoma biomarker [29,30] in breast tissues and compare the results with those of the corresponding HRP-IHC staining. Tn antigen is a truncated O-linked core glycan linked to the serine or threonine of mucin 1 (MUC1) [31–35]. It is a tumor-associated carbohydrate antigen (TACA) present only on epithelial cancer cells due to the lack of the elongation of the core glycan by β1-3 D-galactosyltransferase and α2-6 sialyltransferase enzymes [36,37]. That is, in normal cells Tn antigen is hidden by the additional sugar residues attached to it whereas Tn antigen is exposed in cancer cells. Tn antigen has been observed in more than 90% of human epithelial cancers [38–41]. Tn antigen has been shown to be present in most breast cancers including invasive ductal carcinomas (IDC), invasive lobular carcinomas (ILC) and ductal carcinomas *in situ* (DCIS) [30,42] but absent in a broad range of normal adult tissues including normal breast tissues [43–46]. Tn antigen is also present in some benign breast lesions such as atypical ductal hyperplasia (ADH). However, ADH is considered a cancer precursor [42,44].

We will quantitatively determine the sensitivity and specificity of the AQD-based IF imaging in differentiating breast cancer against normal breast tissues and benign breast tumors and compare these results with those of the corresponding HRP-based IHC probes. Both the AQD IF and the HRP IHC methods will be tested on the same tissue microarrays (TMAs) of breast tissues from 115 patients including 58 malignant cases (stages 0-III) and 57 benign cases. For the AQD-based IF imaging, we will use MPA-capped CdSe AQDs each conjugated to 3.4 SA [24] as the fluorescent label for a three-step indirect staining strategy consisting of (1) binding of the primary antibody to the cancer cells, (2) binding of the biotinylated goat anti-mouse antibody to the primary antibody, and (3) binding of the SA-conjugated AQDs to the biotinylated goat anti-mouse antibody.

2. Materials and methods

2.1. Cell line and cell culture

The MDA-MB-231 (ATCC) is a human breast cancer cell line obtained from Dr. M. J. Reginato of Drexel University of College of Medicine. MDA-MB-231 cells were maintained in DMEM high glucose medium supplemented with 10% fetal bovine serum (Bioexpress, Kaysville, UT), 1% penicillin and streptomycin (Mediatech Inc., Manassas, VA) and cultured at 37 °C in a 5% CO_2 incubator.

2.2. Tissue micro-arrays (TMAs)

Paraffin-embedded tissue blocks from each case were reviewed by co-author, pathologist Linette Mejias (LM), to identify appropriate areas to be included in the TMAs. When an appropriate area was identified, a 2-mm diameter punch was made and the tissue was randomly placed in a TMA block as a core. For each malignant case, we included 3 punches from the malignant region and a punch from the normal breast region. For each benign case, we included three punches from the benign tumor region. A TMA contained 50–60 cores from at least 15 patients randomly distributed within the TMA to minimize potential correlation from core to core. There were a total of 115 patients including 58 breast cancer patients of various breast cancer types and stages and 57 patients with benign breast pathology. There were 395 cores that were successfully made from a total of 403 punches.

2.3. Aqueous quantum dots conjugation

The synthesis of MPA-capped CdSe AQDs followed those of MPA-capped CdS and MPA-capped ZnS [25,47] with an optimal nominal MPA:Cd:Se ratio of 4:3:1 [24]. In what follows all CdSe AQDs were made with this molar ratio. In Fig. 1a we show the photoluminescence excitation (PLE) spectrum (blue) and photoluminescence (PL) spectrum (red) of the CdSe AQDs, which indicates that the peak of the PLE was at 460 nm and the peak of the PL was at 610 nm. In what follows, the window of the excitation filter was 460 ± 20 nm as indicated by the green shade and that of the emission filter was 600 nm long pass as indicated by the orange shade in Fig. 1a. The transmission electron microscopy (JEOL JEM2100) (TEM) image of the CdSe AQD is shown in Fig. 1b which indicated that the CdSe AQDs was crystalline with a size of about 3 nm. Freshly made AQDs suspension was first stored in a refrigerator (4 °C) overnight followed by the removal of the free MPA by centrifugation with a 10 kDa filter (Millipore Co., Beillerica, MA) at 3000 rpm for 10 min three times. After each centrifugation the volume of the suspension was restored by adding pH = 7.0 borate buffer. N-ethyl-N′-dimethylaminopropyl-carbodiimide (EDC) (Thermo Scientific, Rockford, IL, USA) and N-hydroxysuccinimide (NHS) (Thermo Scientific, Rockford, IL, USA) were used to facilitate the peptide bond formation between a primary amine of the SA and a carboxyl on the AQD. First, 4 mg of EDC and 6 mg of NHS were dissolved in 1 ml of 0.1 M 2-(*N*-morpholino)ethanesulfonic acid (MES) buffer (TEKNOVA, Hollister, CA) at pH = 6.5. 2 mM of EDC and 5 mM of NHS were added to the suspension of the AQDs at 1.07 μM particle concentration at pH = 7.0 in borate buffer. The reaction was incubated for 15 min at room temperature followed by the addition of 2-mercaptoethanol (20 mM) to quench the EDC. The suspension was then run through a desalting column (Zeba Spin 7 KW, Pierce, Rockford, IL, USA) to remove unbound reagents and electrolytes in the suspension. The suspension was then mixed with an SA solution at room temperature and pH = 7.0 for 2 h. The unused NHS esters bound on the AQD surface were then quenched by hydroxylamine hydrochloride (10 mM) (Sigma–Aldrich, St. Louis, MO, USA). Unconjugated AQDs and SAs were then removed by microcentrifugation at 12,000 rpm with a 100 kDa filter (Millipore) for 5 min five times. After each microcentrifugation, the volume of the suspension was restored with a 50 mM borate buffer solution of pH 8.3. After five consecutive microcentrifugations, the suspension was filtered through a syringe

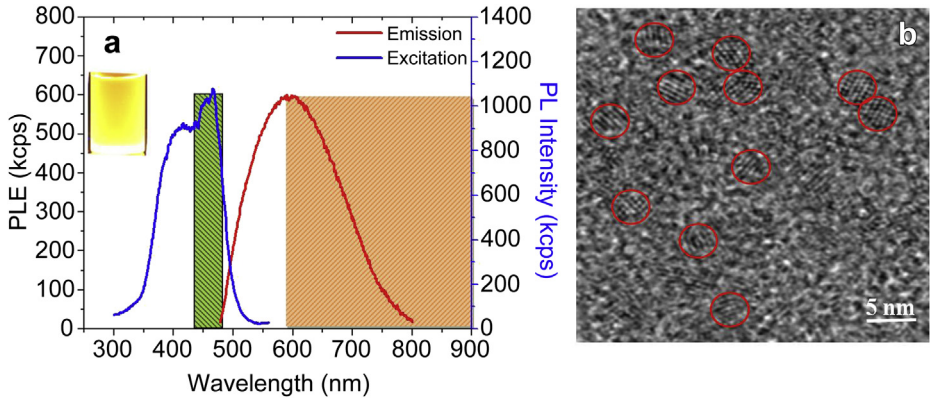

Fig. 1. a) Photoluminescence (PL) spectrum: Emission wavelength peak 460 nm and emission wavelength peak 610 nm, insert is the color of CdSe AQDs under UV-light; The shaded boxes indicate the filter set applied for imaging. Excitation filter is 460 ± 20 nm (green box) and Emission filter is 600 nm long pass (orange box). b) TEM image of AQDs, the particle size is about 3 nm. (For interpretation of the references to color in this figure legend, the reader is referred to the web version of this article.)

with a 0.2 μm filter (Fisherbrand, Newark, DE) to remove large aggregates if any. The conjugated SA-AQD probes were then stored at 4 °C before use.

2.4. AQD – IF staining

2.4.1. Cell line validation of SA-AQD probes

To test the staining capability of the SA-AQD probes, MDA-MB-231 (a human breast cancer cell line) cells were grown on cover glass overnight and then fixed with 4% paraformaldehyde for 15 min. Cells were washed with phosphate buffer saline (PBS) solution three times. Cells were blocked with 10% normal goat serum for 1 h at room temperature to minimize nonspecific binding. Cells were then washed with 0.1% Tween/Tris buffer saline (TBS) 3 times and incubated with mouse anti-Tn antigen antibody (1:25 dilution, Tn218 Genetex, CA) for 1 h at room temperature. Next, they were washed with TBS 3 times for 5 min each and incubated with biotinylated goat anti-mouse IgG/IgM (1:50 dilution, Invitrogen, OR) for 30 min at room temperature followed by TBS wash. They were then incubated with SA-AQD probes for 30 min at room temperature followed by washing with TBS for 3 times and then mounted with DAPI (Mounting medium with fluorescence, Vector Laboratories, CA, USA) for nucleus staining. Samples were stored in the dark at 4 °C. A negative control was a sample undergoing all the steps except the primary antibody step. After staining, the cells were then observed using an Olympus BX51 fluorescent microscope.

2.4.2. TMAs IF staining

TMAs were cut into 5 μm sections, mounted on glass slides, and stained for Tn antigen as follows. Following paraffin removal, hydration, and antigen retrieval in sodium citrate (pH = 6, Thermo Scientific, NJ) at 95 °C for 20 min, the sections were treated with 10% normal goat serum (Vector Laboratories, Burlingame, CA, USA) in 0.1% Tween Tris buffer saline (TBS) solution for 1 h to block nonspecific binding followed by washing in TBS for 3 times, 5 min each. They were then treated with streptavidin (Streptavidin/Biotin Blocking Kit, Vector Laboratories) for 15 min to block potential streptavidin binding to existing biotin in the tissues followed by TBS wash. They were then treated with biotin for 15 min (Streptavidin/Biotin Blocking Kit, Vector Laboratories) to block potential binding of biotinylated antibody to the blocking streptavidin. The slides were then incubated with mouse anti-Tn antigen antibody (1:25 dilution, Genetex, CA) for 1 h at room temperature. Next, they were washed with TBS 3 times each for 5 min. They were then incubated with biotinylated goat anti-mouse IgG/IgM (1:50 dilution, Invitrogen, OR) for 30 min at room temperature, followed by TBS wash. After that, they were incubated with SA-AQD probes for 30 min followed by washing with TBS, counterstaining, and mounting with DAPI mounting medium (Vector Laboratories, Burlingame, CA, USA).

2.5. HRP-IHC staining of TMAs

Prior to HRP staining, the TMA slides went through the same goat serum, streptavidin, and biotin blocking steps as described above. Following that they went through an additional 0.3% hydrogen peroxide (Fisher, Allentown, PA) blocking step for 15 min prior to incubation with mouse anti-Tn antigen antibody (1:25) for 1 h at room temperature. They were then washed by TBS and treated with biotinylated goat anti-mouse IgG/IgM (1:50 dilution, Invitrogen, OR) for 30 min at room temperature. They were then washed by TBS followed by incubation with SA-HRP probes for 30 min. The slides were then washed with TBS and incubated with 3,3′-diamiobenzidine (DAB) for 5 min followed by TBS wash and counterstaining with hematoxylin.

2.6. Imaging, analysis and quantification

The AQD-stained IF slides and the standard HRP-stained IHC slides were examined using a BX51microscope (Olympus) in the fluorescent mode and in the bright field mode, respectively. A MicroVista charge-coupled device (CCD) camera (Intevac, Carlsbad, CA) was mounted on the microscope to take the image. For CdSe AQD imaging, we chose an excitation filter with a wavelength window of 460 nm ± 20 nm (Chroma, Bellows Falls, VT) and a 600-nm long-pass emission filter to allow any emission with a wavelength longer than 600 nm as illustrated respectively by the green and orange shades in Fig. 1(a). For Cy3-labeled SA, a 550-nm excitation filter and a 570-nm emission filer were used.

NIH ImageJ was used to analyze the images of the AQD-stained slides. For each core, six images were taken from different areas of the core. Therefore, for each malignant case there were a total of 18 images from three tumor cores and 6 images from one normal-tissue core. For each benign case, there were 18 images from three tumor cores. In each tissue array, there was a placebo (unstained) heart tissue core. For any fluorescent image analysis, the placebo was first examined to determine the baseline background auto-fluorescent intensity. This baseline background fluorescent intensity was then subtracted from those of all the images to minimize the contribution from autofluorescence. After the background subtraction, the fluorescent intensity per unit area (FPA) of each cell was then determined within the area of that cell using ImageJ, which we defined as the cellular fluorescent intensity per unit area (CFPA). CFPA was then recorded for each cell. A histogram of CFPA was then constructed over 500–700 cells from micrographs taken from six different regions of each core, from which the average CFPA of that core was then computed. The average CFPA of each core was then recorded as the quantitative CFPA of that core. After the AQD staining results were reported to the pathologist (LM), the disease status of each core of the TMAs was then unblinded and the reported CFPA of each core was compared to the disease status of the core. With this comparison, the numbers of true positives, true negatives, false positives, and false negatives were obtained to calculate the sensitivity and specificity of the AQD imaging both by core and by case. A receiver operating characteristic (ROC)–sensitivity versus (1-specificity)–curve was also constructed. The area under the ROC curve represents the diagnostic accuracy [48]. Student *t*-test was then carried out for analysis with 95% confidence if the signals from the malignant cores were statistically different from those of the normal cores and if the signals of the benign cores were the same as those of the normal cores. ANOVA test was carried out to analyze if Tn antigen expression level varied with cancer grade or type.

3. Results and discussions

3.1. SA-AQD probes staining of MDA-MB-231 cells

As an example of AQD staining of Tn antigen expression in breast cancer cells, AQD-Tn stained MDA-MB-231 cancer cells using the method described above are shown in Fig. 2a. The presence of Tn antigen on the MDA-MB-231 cells was evident by the strong AQD-Tn staining of the cells. For comparison, MDA-MB-231 cells were also stained by Cy3-labeled SA and shown in Fig. 2b. As can be seen, both SA-AQD and SA-Cy3 showed strong fluorescent signals on the cancer cells while the negative control (Fig. 2c)–which underwent all the AQD staining steps except the primary antibody

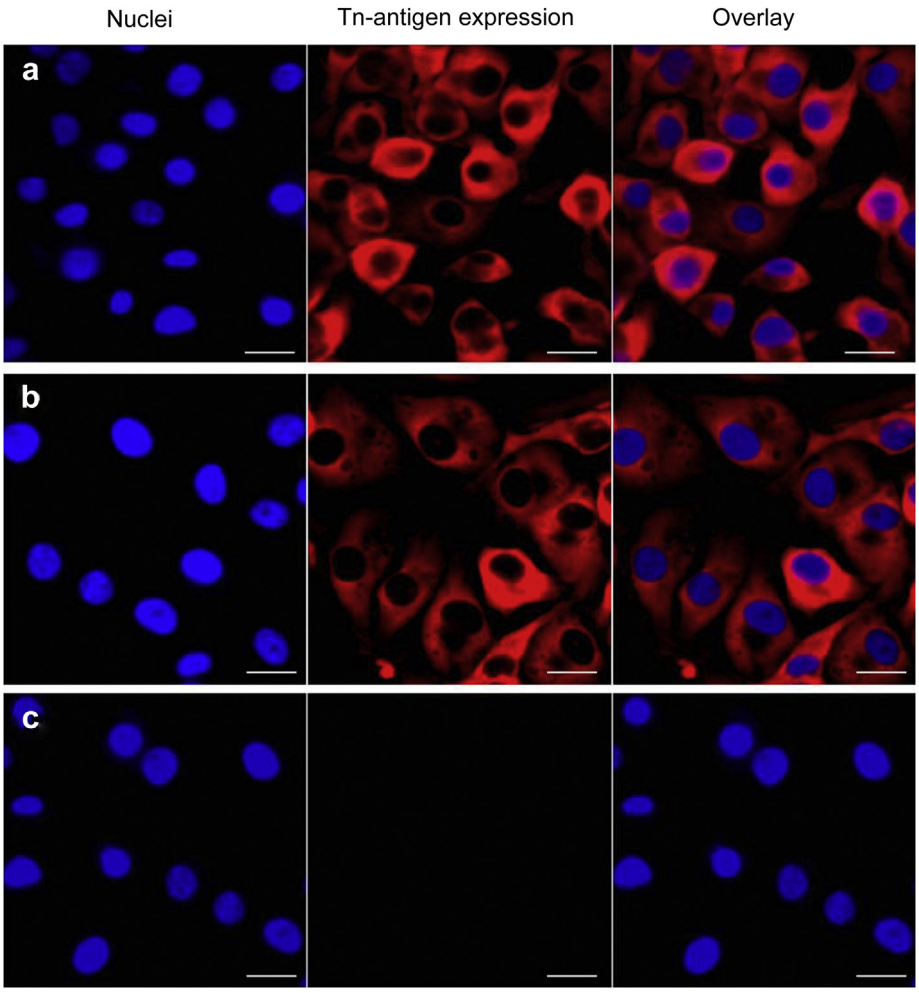

Fig. 2. Immunofluorescent staining of MDA-MB-231 cells for Tn antigen expression. (a) MDA-MB-231 cells stained with AQD-SA complexes; (b) MDA-MB-231 cells stained with Cy3-SA (c) negative control, without primary antibody. Tn antigen expression was mostly on the membrane and in cytoplasm. Scale bar: 30 μm.

step–showed no fluorescent signals. Furthermore, AQD-stained cells exhibited stronger fluorescent signals than Cy3-stained cells using the same concentrations of the antibodies, indicating that AQDs were better fluorescent labels than Cy3. The better fluorescent labeling performance of the AQDs may be due to several reasons. Firstly, AQDs were nanoparticles which had the capability to emit more than one photon at a time thus theoretically could be brighter than Cy3 which was only a molecule. Secondly, the separation of the excitation wavelength and the emission wavelength of the AQDs was more than 100 nm, which had the advantage of minimal interference between the excitation and emission whereas Cy3 had an excitation and emission wavelength separation of less than 20 nm and its emission was likely to have interference from the excitation [49]. Thirdly, the 600 nm long-pass filter used only the red and the near infrared (NIR) part of the AQD emission spectrum where autofluorescence of the paraffin-embedded tissues fell off sharply [50]. These attributes permitted the AQDs to minimize background noise in imaging paraffin-embedded tissues [51].

3.2. AQD staining and HRP staining of TMAs

Examples of the AQD-Tn staining of a Stage II IDC (column 1), a Stage III IDC (column 2), and a benign breast condition of ductal hyperplasia without atypia (column 3) are shown in Fig. 3a. The HRP-Tn staining and the hematoxylin and eosin (H&E) staining of the same tissues are shown in Fig. 3b and c, respectively. As can be seen from Fig. 3a and b, both the AQD staining and the HRP staining showed intense expression of Tn antigen in the cytoplasm and the cell membrane of the IDC cores (columns 1 and 2), which were typical of most of the AQD IF staining and HRP IHC staining of malignant cores. In contrast, the normal cores of the breast cancer cases and the benign cores generally showed little Tn antigen expression. However, HRP-Tn staining exhibited more false positives than AQD-Tn staining. As an example, we showed the AQD-Tn staining, HRP-Tn staining and H&E staining of a ductal hyperplasia without atypia in the third column of Fig. 3a, b, and c, respectively. As can be seen, AQD-Tn staining correctly showed no Tn antigen expression whereas the HRP-Tn staining was falsely positive of Tn antigen expression.

3.3. Quantitative analysis of AQD staining

The average cellular fluorescent intensity per unit area (CFPA) of the AQD-Tn staining by case of all the 115 cases was summarized in Fig. 4a where red solid symbols (in web version) represent malignant tumors, green solid symbols benign conditions and blue open symbols the normal cores of the malignant cases. As can be seen in Fig. 4a, the CFPA for the normal cores of the malignant cases were mostly below 20 whereas the CFPA of the malignant tumors were

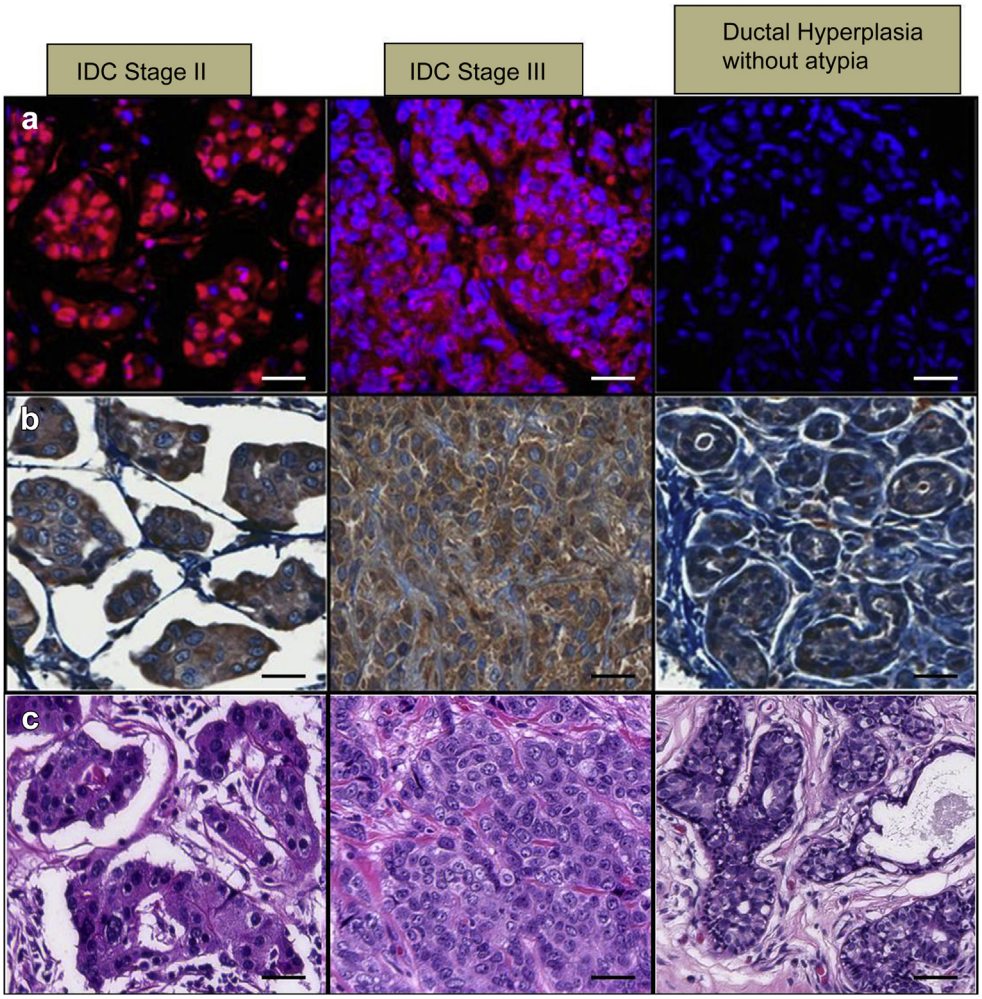

Fig. 3. Tn antigen expression in invasive ductal carcinomas and benign changes. (a) AQD-IF staining. Strong staining of all cells was observed for both IDC Stage II and IDC Stage III. No staining was observed in AQD-stained section for Ductal hyperplasia without atypia. (b) Corresponding HRP IHC staining for the same section: Strong staining of all cells for both IDC Stage II and IDC Stage III as well as Ductal hyperplasia without atypia. (c) H&E images of the same case. AQD IF staining is more specific than HRP IHC staining method. AQD-IF stained sections, blue: nuclei, red: Tn antigen. Scale bars: 200 μm.

well above 20. The CFPAs of most of the benign cores were also below 20 as similar to those of the normal cores of the malignant cases. This indicates that AQD-Tn antigen was sensitive and specific in differentiating cancers from the normal breast tissues and the benign conditions.

Based on the results shown in Fig. 4a, we plot in Fig. 4b the CFPA histogram for the malignant tumors (red open circles), benign tumors (green open circles), and the normal tissues of the malignant cases (blue open circles). The histograms were then fitted to a log-normal distribution using MATLAB. Also shown in Fig. 4b are the fitted log-normal CFPA distribution of the malignant tumors (red solid line), that of the normal tissues of the malignant cases (blue solid line), and that for the benign lesions (green solid line). As can be seen, the CFPA distribution of the malignant tumors was well distanced from that of the normal tissues and that of the benign lesions with a small overlap near CFPA = 20. Using a threshold of CFPA = 20, we obtained a p value of 0.0036 between malignant tumor and normal tissue, indicating that malignant tumors were indeed different from the normal tissues. On the other hand, with the same CFPA threshold of =20, we obtained a p value of 0.059 between the benign tumors and the normal tissues, indicating that there was no difference between the normal tissues of the malignant cases and the benign tumors. In what follows, all the statistics of the AQD-Tn staining was based on a cutoff CFPA of 20 and that of the HRP-Tn staining was based on the conventional scoring system where the prediction of each core was based on the pathologist's judgment of the staining instead of the quantitative analysis for the AQD-based staining shown above.

Sensitivity versus (1-specificity) receiver operating characteristic (ROC) curve for the AQD-Tn staining is shown in Fig. 4c. The area under the ROC curve represents the accuracy of the malignancy decision. An area of unity represents a perfect prediction. The area under the ROC curve of the AQD-Tn staining in Fig. 4c was 0.97 whereas the area under the ROC curve for the HRP-Tn staining (not shown) was 0.89, indicating that overall Tn antigen staining was a good tool to differentiate breast cancer from normal breast tissues and benign breast conditions and that AQD-Tn staining was better than HRP-Tn staining.

The sensitivity and specificity of AQD-Tn staining and those of HRP-Tn staining for differentiating breast cancer from normal breast tissues and benign breast conditions are summarized in Table 1. As can be seen, AQD-Tn staining exhibited 95% sensitivity and 90% specificity whereas HRP-Tn staining exhibited 90% sensitivity and 80% specificity, confirming that AQD-Tn staining provided better sensitivity and specificity than HRP-Tn staining to detect breast cancer against normal breast tissues and benign

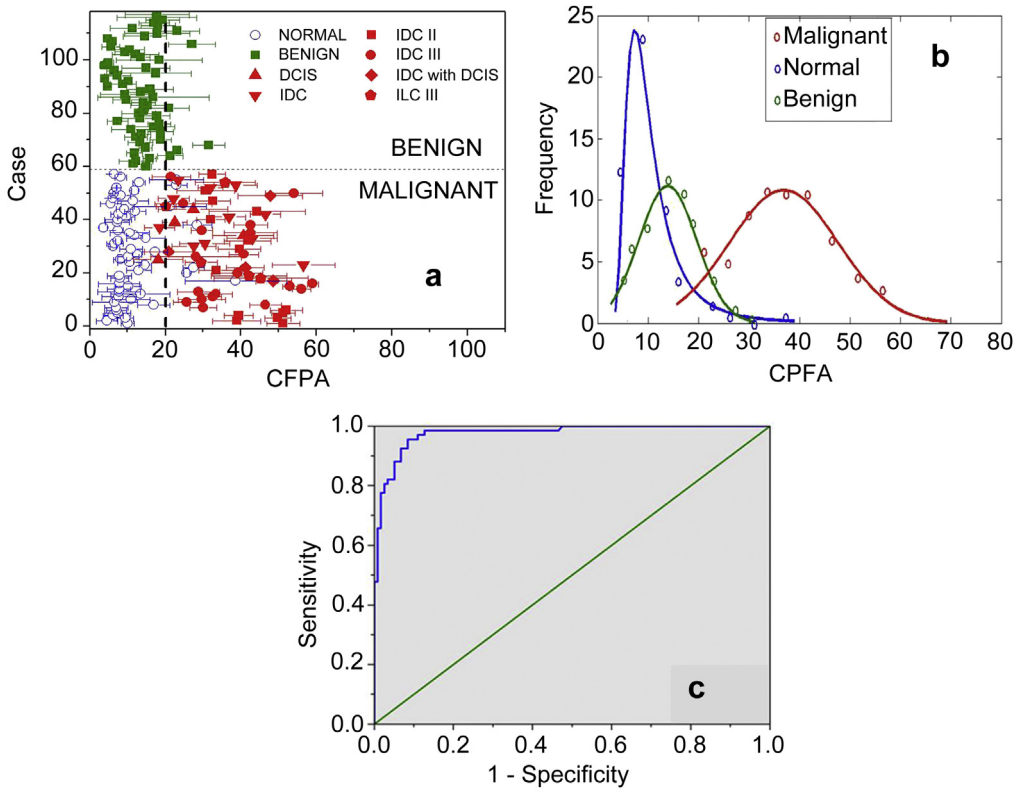

Fig. 4. (a) Fluorescent Intensity of AQD-stained sections of 115 cases for Tn antigen expression; (b) Tn antigen frequency distribution; (c) ROC curve of cancer detection using Tn antigen as marker. Normal vs. Malignant $p = 0.0036$; Normal vs. Benign $p = 0.059$. Area under ROC curve is 0.976 (95% CI 0.956–0.995).

breast conditions. In addition, the 95% sensitivity obtained by the AQD staining was also better than the 90% sensitivity and 77% specificity obtained by Springer earlier [52]. The reason that the AQD-Tn staining was highly sensitive and specific in differentiating breast cancer against normal breast tissues and benign breast conditions was due to the combination of the facts that Tn antigen was specific to epithelial cancers and that the present AQD staining avoided much of interference by auto-fluorescence.

It is also of interest to note that in contrast to the quantitative analysis of the AQD-staining as discussed above, the analyses of HRP stained sections relied on visual scoring [1] of high, moderate or weak staining. It was often difficult to distinguish the true signal from the background signal. Although there have been many scoring systems introduced such as the Allred score [53], interpretation of HRP staining still depends on the experience and skill of the pathologists. A study in Germany involving 172 pathologists to assess estrogen receptor staining resulted in 24% false-negative assessment [54]. As shown above the analysis of AQD-stained sections was quantitative and did not require visual scoring by a highly trained pathologist and was more sensitive and specific than the HRP staining.

The sensitivity and specificity of the AQD-Tn staining also prevailed on the cellular level. The average CFPA and the percentage of the cells positive of the AQD-Tn staining of various tissue types are summarized in Table 2. As can be seen, all breast cancers regardless of cancer type and cancer stage exhibited a high CFPA well over 20 and the percentage of cells that was positive by AQD-Tn staining was high (>90%) for all breast cancers. In contrast, the average CFPA of the normal tissues and that of the benign conditions were well below 20 and there was a low percentage (mostly below 10%) of cells stained positive by AQD-Tn. This indicates that AQD-Tn staining was not only sensitive and specific in detecting breast cancer but was also uniform in imaging breast cancer. It is worth noting that the present AQD-Tn staining did not exhibit much fluorescent signal above the cutoff for the majority of the benign cases and normal breast tissues, which is different from earlier findings [34], presumably due to the advantageous attributes of the AQDs stated above.

How the Tn expression varied with cancer type, stage and grade was also examined within the 58 malignant cases. A summary of the average CFPA versus cancer stage including both lobular and ductal carcinomas for all 58 malignant cases is shown in Fig. 5a. A summary of the average CFPA versus cancer grade is shown in Fig. 5b. As can be seen from Fig. 5a, the intensity of the AQD-Tn staining did not vary much across different cancer stages or cancer types. An ANOVA test was carried out and showed a p-value of 0.76 among all 58 cases, indicating that Tn antigen expression was independent of cancer stages. As examples, we show the AQD-Tn

Table 1
Comparison of the sensitivity and specificity of (a) AQD staining and (b) HRP staining of Tn antigen for detecting breast cancer.

(a)	Pathologic malignant	Pathologic benign
AQD-IF positive	55	6
AQD-IF negative	3	51
Total Cases	58	57
Sensitivity	**95%**	
Specificity	**90%**	

(b)	Pathologic malignant	Pathologic benign
HRP IHC positive	52	11
HRP IHC negative	6	50
Total Cases	58	57
Sensitivity	**90%**	
Specificity	**80%**	

Table 2
CFPA and percentage of cells positive of AQD-Tn staining in various types of breast cancer tissues (including DCIS, IDC, and ILC), normal breast tissues (including both the normal tissues of malignant cases and benign conditions with no pathological changes), and benign breast conditions with pathological changes.

Tissue type		# of cases	CFPA	% Of cells positive of AQD-Tn stain
DCIS		4	18–41	95 ± 5%
IDC	IDC with DCIS	4	21–48	92 ± 2%
	Stage I	11	28–57	98 ± 3%
	Stage II	14	31–52	91 ± 6%
	Stage III	19	22–59	90 ± 3%
ILC	Stage II	1	31	95 ± 2%
	Stage III	4	20–45	91 ± 3%
Normal breast tissues		74	6–18	3 ± 5%
Benign changes	Stromal Fibrosis	11	7–18	5 ± 3%
	Fibroadenoma	7	13–23	20 ± 10%
	Hyperplasia without atypia	10	7–23	10 ± 12%
	Apocrine metaplasia	5	13–17	3 ± 4%
	Adenomyepithelioma	1	13	4 ± 3%
	Papiloma intraductal	2	16–18	6 ± 2%
	Ductal ectasia	4	4–13	5 ± 4%
	Acute inflammation	1	7	0
	Sclerosing adenosis	1	18	7 ± 2%

staining, HRP-staining, and H&E staining of a DCIS (column1), stage-I IDC (column 2), stage-II ILC (column 3), and stage-III ILC (column 4) in Fig. 6a, b, and c, respectively. As can be seen, the Tn antigen expression level indeed did not vary much between different cancer types and stages (Fig. 6).

In contrast, Fig. 5b suggests that Tn antigen expression increased with cancer grade. Note that the grade information was not always provided on the pathology reports for earlier cases. Only 10 out of the 58 malignant cases had grade information. Even though there were only 10 cases, an ANOVA test carried out with these 10 cases showed a p value of 0.04. Although 10 cases were a small number, it nonetheless supported that the level of CFPA had correlation with grade. As examples, in Fig. 7a we shows the AQD-Tn staining of a grade-1 IDC (column 1), a grade-2 IDC (column 2), and a grade-3 IDC (column 3). The corresponding H&E staining of the same tissues was shown in Fig. 7b. These AQD-Tn staining images support the notion that Tn antigen expression level increased with an increasing grade. This was consistent with the finding of Springer et al. [55] that Tn expression was correlated with the aggressiveness of the cancer.

3.4. Durability of AQD stained slides

Immunofluorescent staining is a well-studied technique and widely used in the biomedical field. However, currently available organic fluorescent dyes such as Alexa Fluor and Cyanine will photobleach rapidly and irreversibly under intense illumination, rendering them unsuitable for many clinical applications. QDs do not photo-bleach over a significant period of time. In this study, we have examined the stability of the AQD-stained slides. All slides were stored in the refrigerator (4 °C) and wrapped in an aluminum foil. The slides were periodically examined for the average CFPA. As an example, the fluorescent images of a slide right after staining, 6 months, and 10 months after staining are shown in Fig. 8a, b, c, respectively. As can be seen, even after 10 months, the fluorescent image was still almost as good as that obtained right after staining. In Fig. 8d, we plot the average CPFA versus storage time of 7 slides that had been stored for the longest time. As can be seen, even after 10 months of storage and periodic examinations under strong light, the average CFPA after 6 months still retained better than 90% of the initial CFPA and there was no further change after 6th month. Such durability suggests that AQD-based staining can be a good tool for molecular pathological applications. Furthermore, unlike organic dyes, protection from light was not necessary during laboratory processes. This further makes AQD-based staining attractive for molecular pathological examination.

3.5. Macroscopic visualization of breast cancer by AQD staining

It is of interest to note that on a macroscopic scale, the fluorescent image of the AQD staining could also be easily seen by unaided human eyes. As an example, the fluorescent image of a slide containing an entire AQD-stained tissue array when placed under a UV lamp and captured by a consumer camera is shown in Fig. 9a where each core was 2 mm in size. An H&E stained slide of the same tissue array is shown in Fig. 9b. As can be seen in Fig. 9a, only the malignant cores were visible in the fluorescent image. The yellow circles indicate the normal cores that were invisible in the fluorescent image. There were some missing cores (white circles) which were lost during the sectioning of the block. The fact that malignant cores were easy to observe without any magnification and that there was no observable loss of signal during a continuous light exposure indicate that AQDs were an excellent fluorescent label and that Tn antigen was a specific and sensitive marker to distinguish breast cancer from normal breast tissues.

4. Conclusion

In this study, we have examined the use of CdSe AQDs each conjugated to three streptavidin as a fluorescent label to image Tn antigen expression in various breast tissues via a sandwich staining procedure where the primary monoclonal anti-Tn antibody was

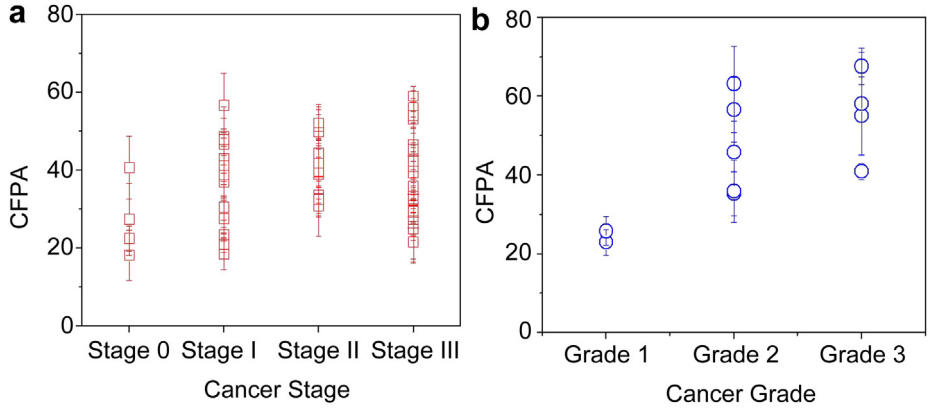

Fig. 5. (a) CFPA of AQD-stained sections of 58 cases for Tn antigen expression according to cancer stages (including both ductal and lobular types), p value = 0.76; (b) Tn antigen expression according to cancer grades, p value = 0.04. A total of 10 cases with different cancer stages were included.

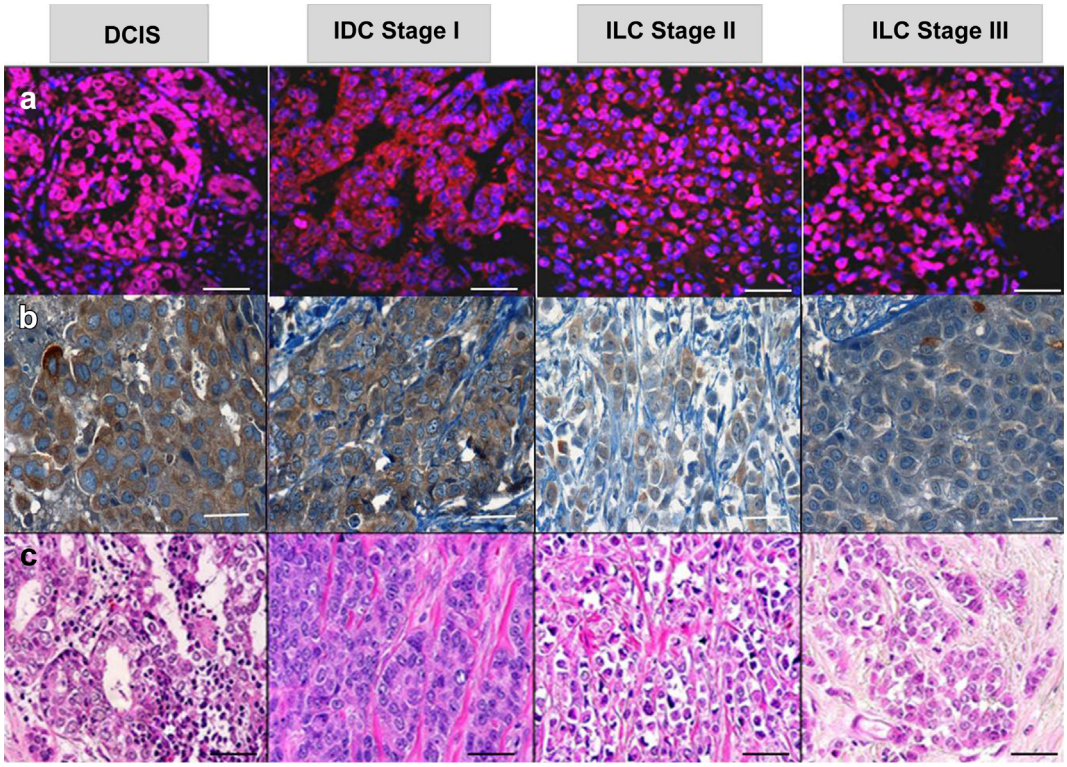

Fig. 6. (a) AQD-Tn staining, (b) HRP-Tn staining, and (c) H&E staining of a DCIS (column1), stage-I IDC (column 2), stage-II ILC (column 3), and stage-III ILC (column 4) Note Tn antigen expression level did not vary much between different cancer types and stages. Scale bars: 200 μm.

bound to the Tn antigen on the tissue, a biotin-labeled secondary antibody was bound to the primary anti-Tn antibody, and finally the streptavidin conjugated AQDs were bound to the biotin on the secondary antibody. We have evaluated the AQD staining of Tn antigen on tissue microarrays of a total of 395 cores from 115 cases including various breast cancer cores, normal tissues cores from breast cancer patients and benign breast tumor cores and compared to HRP-based staining of the same tissues. We showed that AQD-Tn staining was positive for more than 90% of the breast cancer cells but not for cells in the normal breast tissues and benign breast tumors. The AQD-Tn staining exhibited 95% sensitivity and 90% specificity which were better than the 90% sensitivity and 80% specificity exhibited by the HRP staining using the same antibodies on the same tissues and prior fluorescent imaging studies of Tn antigen of breast cancer in

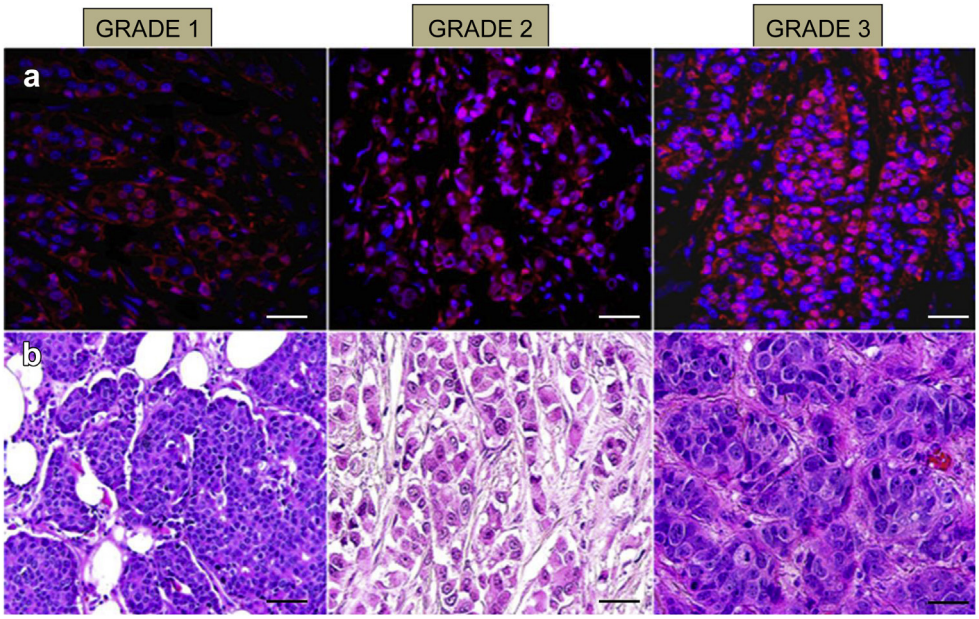

Fig. 7. (a) AQD-Tn staining and (b) H&E staining of a grade-1 IDC (column 1), a grade-2 IDC (column 2) and a grade-3 IDC (column 3). Note Tn expression increased notably with grade. Scale bars: 200 μm.

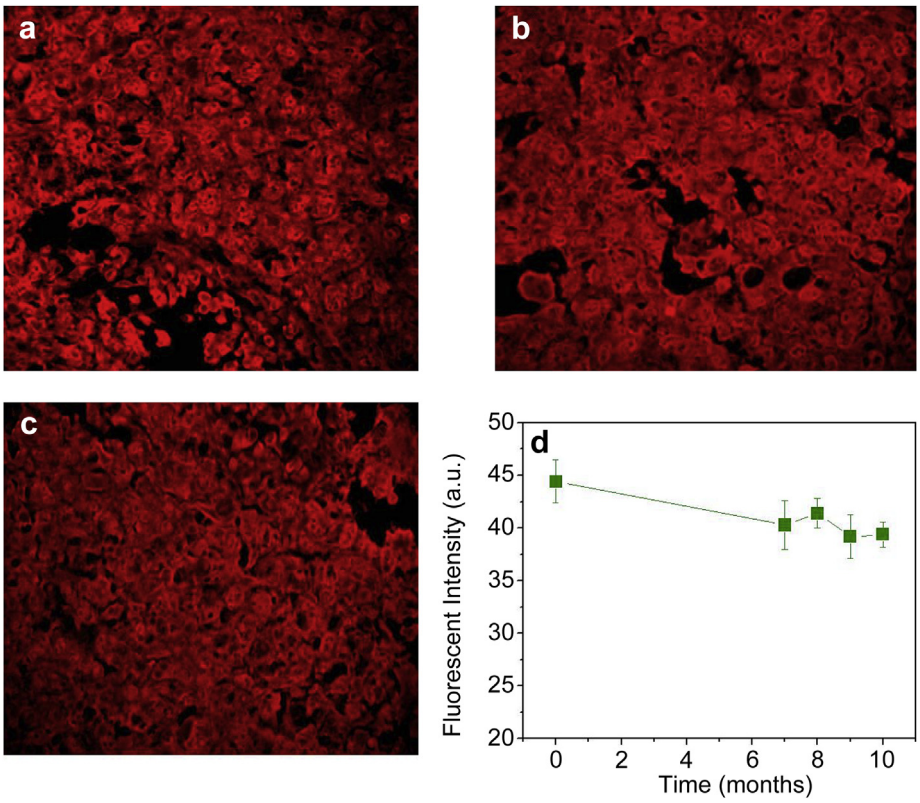

Fig. 8. Stability of AQD-probe for imaging Tn antigen expression in breast cancer tissue. (a) Image was taken right after staining procedure; (b) image was taken after 6-month storage (4 °C); (c) image was taken after 10-month storage (4 °C); (d) quantitative fluorescent intensity signal over different periods of time.

the literature. We also showed that the CFPA of AQD-Tn staining could be correlated with tumor grade but independent of cancer type and stage as consistent with the earlier report that Tn antigen was associated with tumor aggressiveness, invasion, and spreading but independent of tumor stage and type. In addition to better sensitivity and specificity, AQD-based imaging is also quantitative with a well-defined cutoff as compared to the qualitative visual determination of the conventional IHC staining method.

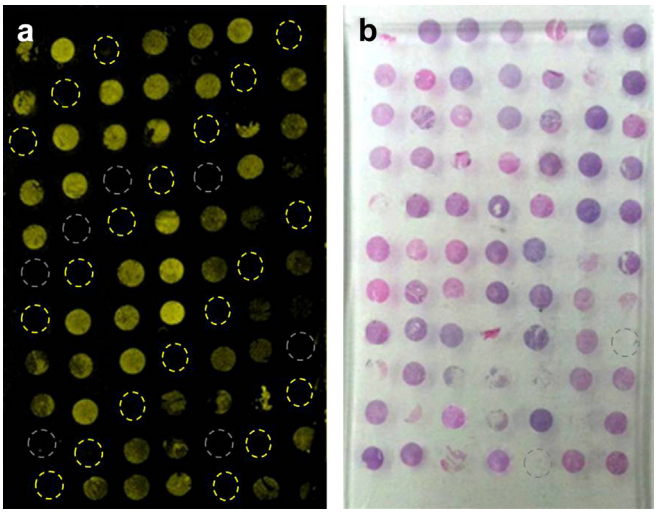

Fig. 9. Entire TMA consists of cores from 19 cancer cases. (a) TMA under UV light; (b) H&E stained section. Cancer cores showed fluorescent signal that could be detected with naked eyes while benign cores didn't show visible signal. Yellow-dotted circles are benign cores. Gray circles are missing core due to cutting of the section. (For interpretation of the references to color in this figure legend, the reader is referred to the web version of this article.)

Acknowledgment

This work is supported in part by the Grants W81XWH-09-1-0701 of Department of Defense and the Drexel University-Wallace Coulter Foundation Partnership. The authors would also like to thank Dr. M. J. Reginato of Drexel University of College of Medicine for providing us with the MDA-MB-231 cell line.

References

[1] Walker RA. Quantification of immunohistochemistry – issues concerning methods, utility and semiquantitative assessment I. Histopathology 2006;49(4):406–10.
[2] Cregger M, Berger AJ, Rimm DL. Immunohistochemistry and quantitative analysis of protein expression. Arch Pathol Lab Med 2006;130:1026–30.
[3] Fritz P, Wu X, Tuczek H, Multhaupt H, Schwarzmann P. Quantitation in immunohistochemistry. A research method or a diagnostic tool in surgical pathology? Pathologica 1995;87:300–9.
[4] McCabe A, Dolled-Filhart M, Camp RL, Rimm DL. Automated quantitative analysis (AQA) of in situ protein expression, antibody concentration adn prognosis. J Natl Cancer Inst 2005;97:1808–15.
[5] Szeszel MK, Crisman CL, Crow L, McMullen S, Major JM, Natarajan L, et al. Quantifying estrogen and progesterone receptor expression in breast cancer by digital imaging. J Histochem Cytochem 2005;53(6):753–62.
[6] Baschong W, Suetterlin R, Laeng RH. Control autofluorescence of archival formaldehyde-fixed, paraffin-embedded tissue in confocal laser scanning microscopy (CLSM). J Histochem Cytochem 2001;49:1565–72.
[7] Chen H, Xue J, Zhang Y, Zhu X, Gao J, Yu B. Comparison of quantum dots immunofluorescence histochemistry and conventional immunohistochemistry for detection of caveolin-1 and PCNA in the lung cancer tissue microarray. J Mol Hist 2009;40:261–8.
[8] Zhou M, Ghosh I. Quantum dots and peptides: a bright future together. Biopolymers 2007;88(3):325–39.
[9] Watanabe M, Fujioka K, Akiyama N, Takeyama H, Manabe N, Yamamoto K, et al. Conjugation of quantum dots and JT95 IgM monoclonal antibody for

thyroid carcinoma without abolishing the specificity and activity of the antibody. IEEE Trans Nanobiosci 2011;10(1):30–6.
[10] Xia Z, Xing Y, So MK, Koh AL, SInclair R, Rao J. Multiplex detection of protease activity with quantum dot nano sensors prepared by intermediated specific bioconjugation. Anal Chem 2008;80:8649–55.
[11] Wu X, Liu H, Liu J, Haley KN, Treadway JA, Larson JP, et al. Immunofluorescent labeling of cancer marker Her2 and other cellular targets with semiconductor quantum dots. Nat Biotechnol 2003;21:41–6.
[12] Jaiswal JK, Goldman ER, Mattoussi H, Simon SM. Use of quantum dots for live cell imaging. Nat Methods 2004;1:73–8.
[13] Wu CS, Oo MKK, Cupps JM, Fan X. Robust silica-coated quantum dot-molecular beacon for highly sensitive DNA detection. Biosens Bioelectron 2011;26:3870.
[14] Kim S, Lim YT, Soltesz EG, De Grand AM, Lee J, Nakayama A, et al. Near-infrared fluorescence type II quantum dots for sentinel lymph node mapping. Nat Biotechnol 2004;22:93–7.
[15] Wang J, Yong WH, Sun Y, Vemier PT, Koeffler HP, Gundersen MA, et al. Receptor-targeted quantum dots: fluorescent probes for brain tumor diagnosis. J Biomed Opt 2007;12:044021.
[16] Zhang CY, Hu J. Single quantum dot-based nanosensor for multiple DNA detection. Anal Chem 2010;82(5):1921–7.
[17] Cady NC. Quantum dot molecular beacons for DNA detection. Mehods Mol Biol 2009;544(3):367–79.
[18] Kim JH, Chaudhary S, Ozkan M. Multicolor hybrid nanoprobes of molecular beacon conjugated quantum dots: FRET and gel electrophoresis assisted target DNA detection. Nanotechnology 2007;18:195105.
[19] Papagiannaros A, Upponi J, Hartner W, Mongayt D, Levchenko T, Torchilin V. Quantum dot loaded immunomicelles for tumor imaging. BMC Med Imaging 2010;10:22–31.
[20] Jiang W, Papa E, Fischer H, Mardyani S, Chan WC. Semiconductor quantum dots as contract agents for whole animal imaging. Trends Biotechnol 2004;22:607–9.
[21] Chen C, Peng J, Xia H, Yang GF, Wu QS, Chen LD, et al. Quantum dots-based immunofluorescence technology for the quantitative determination of Her2 expression in breast cancer. Biomaterials 2009;30:2912–8.
[22] Chen C, Xia HS, Gong YP, Peng J, Hu MB, Zhu XB, et al. The quantitative detection of total HER2 load by quantum dots and the identification of a new subtype of breast cancer with different 5-year prognosis. Biomaterials 2010;31(33):8818–25.
[23] Yang XQ, Chen C, Peng CW, Hou JX, Gong YP, Zhu XB, et al. Quantum dot-based quantitative immunofluorescence detection and spectrum analysis of epidermal growth factor receptor in breast cancer tissue arrays. Int J Nanomed 2011;6:2265–73.
[24] Au GHT, Shih WY, Shih WH. High conjugation efficiency aqueous quantum dots for bioimaging. Analyst 2013;138:7316–25.
[25] Li H, Shih WY, Shih WH. Synthesis and characterization of aqueous carboxyl-capped CdS quantum dots for bioapplications. Ind & Eng Chem Res 2007;46(7):2013–9.
[26] Li H, Shih WY, Shih WH. Non-heavy metal ZnS quantum dots with bright blue photoluminescence by a one-step aqueous synthesis. Nanotechnology 2007;18(20):5604.
[27] Li H, Shih WY, Shih WH. Stable aqueous ZnS quantum dots obtained using (3-mercaptopropyl)trimethoxysilane as a capping molecule. Nanotechnology 2007;18(49):5605.
[28] Li H, Shih WY, Shih WH. Highly photoluminescent and stable aqueous ZnS quantum dots. Ind Eng Chem Res 2010;49:578–82.
[29] Springer GF. T and Tn, general carcinoma autoantigens. Science 1984;224(4654):1198–206.
[30] Springer GF. Immunoreactive T and Tn epitopes in cancer diagnosis, prognosis and immunotherapy. J Mol Med 1997;75(8):594–602.
[31] Galonic DP, Gin DY. Chemical glycosylation in the synthesis of glycoconjugate antitumor vaccines. Nature 2007;446:1000–7.
[32] Solvin SF, Keding SJ, Ragupathi G. Carbohydrate vaccines as immunotherapy for cancer. Immunol Cell Biol 2005;83:418–28.
[33] Ju T, Otto VI, Cummings RD. The Tn antigen – structural simplicity and biological complexity. Angewandte Chemie 2011;50:1770–91.
[34] Konska G, Guerry M, Caldefie-Chezet F, De Latour M, Guillot J. Study of the expression of Tn antigen in different types of human breast cancer cells using VVA-B4 lectin. Oncol Rep 2006;15:305–10.
[35] Li Q, Anver MR, Butcher DO, Gildersleeve JC. Resolving conflicting data on expression of the Tn antigen and implications for clinical trials with cancer vaccines. Mol Cancer Ther 2009;8(4):971–80.
[36] Zuang D, Yousefi S, Dennis JW. Tn antigen and UDP-Gal: GalNAc-Rß1-3-galactosyltranferase expression in human breast carcinoma. Cancer Biochem Biophys 1991;12:185–98.
[37] Ju T, Lanneau GS, Gautam T, Wang Y, Xia B, Stowell SR, et al. Human tumor antigens Tn and sialyl Tn arise from mutations in cosmc. Cancer Res 2008;68(6):1636–46.
[38] Carrilho C, Cantel M, Gouveia P, David L. Simple mucintype carbohydrate antigens (Tn, sialosyl-Tn, T and sialosyl-T) and gp230 mucin-like glycoprotein are candidate markers for neoplastic transformation of the human cervix. Virchows Arch 2000;437:173–9.
[39] Kishikawa T, Ghazizadeh M, Sasaki Y, Springer GF. Specific role of T and Tn tumor-associated antigens in adhesion between a human breast carcinoma cell line and a normal human breast epithelial cell line. Jpn J Cancer Res 1999;90:326–32.
[40] Imai J, Ghazizadeh M, Naito Z, Asano G. Immunohistochemical expression of T, Tn and sialyl-Tn antigens and clinical outcome in human breast carcinoma. Anticancer Res 2001;21:1327–34.
[41] Blixt O, Lavrona OI, Mazurov DV, Clo E, Kracun SK, Bovin NV, et al. Analysis of Tn antigenicity with a panel of new IgM and IgG1 monoclonal antibodies raised against leukemic cells. Glycobiology 2012;22(4):529–42.
[42] Konska G, Guillot J, De Lamour M, Fonck Y. Expression of Tn antigen and N-acetyllactosamine residues in malignant and benign human breast tumors detected by lectins and monoclonal antibody 84D4. Int J Oncol 1998;12:361–7.
[43] Konska G, Vissac C, Zagla K, Chezet F, Vasson MP, Bernard-Gallon D, et al. Ultrastructural localization of binding sites for PNA and VVA-B4 lectins in human breast cancer cell lines detected by confocal fluorescent microscopy. Int J Oncol 2002;21:1009–14.
[44] Demichelis S, Alberdi CG, Servi WJ, Isla-Larrain MT, Segal-Eiras A, Croce MV. Comparative immunohistochemical study of MUC1 and carbohydrate antigens in breast benign disease and normal mammary gland. Appl Immunohistochem Mol Morphol 2010;18:41–50.
[45] Springer GF. Immunoreactive T and Tn epitopes in cancer diagnosis, prognosis, and immunotherapy. J Mol Med 1997;75:594–602.
[46] Desai P. Immunoreactive T and Tn antigen in malignancy: role in carcinoma diagnosis, prognosis, and immunotherapy. Transfus Med Rev 2000;14:312–25.
[47] Li H, Shih WH, Shih WY, Chen L, Tseng SJ, Tang SC. Transfection of aqueous CdS quantum dots using polyethylenimine. Nanotechnology 2008;19:1–8.
[48] Altman DG, Bland JM. Diagnostic tests 3: receiver operating characteristic plots. BMJ 1994;309(6948):188.
[49] Santra S, Dutta D, Walter GA, Moudgil BM. Fluorescent nanoparticle probes for cancer imaging. Technol Cancer Res Treat 2005;4:593–602.
[50] Oliveira VC, Carrara RCV, Simoes DLC, Saggioro FP, Carlotti Jr CG, Covas DT, et al. Sudan Black B treatment reduces autofluorescence and improve resolution of in situ hybridization specific fluorescent signals of brain sections. Histol Histopathol 2010;25:1017–24.
[51] Dahan M. From analog to digital: exploring cell dynamics with single quantum dots. Histochem Cell Biol 2006;125:451–6.
[52] Springer GF. T and Tn pancarcinoma markers: autoantigenic adhesion molecules in pathogenesis, prebiopsy carcinoma-detection, and long-term breast cancinoma immunotherapy. Crit Rev Oncog 1995;6(1):57–85.
[53] Harvey JM, Clark GM, Osborne CK, Allred DC. Estrogen receptor status by immunohistochemistry is superior to the ligand-binding assay for predicting respond to adjuvant endocrine therapy in breast cancer. J Clin Oncol 1999;17:1477–81.
[54] Rudiger T, Hofler H, Kreipe HH, Nizze H, Pfeifer U, Stein H, et al. Quality assurance in immunohistochemistry: results of an interlaboratory trail involving 172 pathologists. Am J Surg Pathol 2002;26(7):873–82.
[55] Springer GF, Desai PR, Ghazizadeh M, Tegtmeyer H. T/Tn pancarcinoma autoantigens: fundamental diagnostic and prognostic aspects. Cancer Detect Prev 1995;19(2):173–82.